Determination of mode II cohesive law of bovine cortical bone using direct and inverse methods

F.A.M. Pereira [a,*], M.F.S.F. de Moura [b], N. Dourado [c], J.J.L. Morais [a], J. Xavier [a], M.I.R. Dias [d]

[a] CITAB/UTAD, Departamento de Engenharias, Quinta de Prados, Vila Real 5001-801, Portugal
[b] Faculdade de Engenharia da Universidade do Porto, Departamento de Engenharia Mecânica, Rua Dr. Roberto Frias, Porto 4200-465, Portugal
[c] CMEMS-UMinho, Departamento de Engenharia Mecânica, Universidade do Minho, Campus de Azurém, Guimarães 4804-533, Portugal
[d] CITAB/UTAD, Departamento de Ciências Veterinárias, Quinta de Prados, Vila Real 5001-801, Portugal

ABSTRACT

This study presents two alternative methods to determine the cohesive law of bovine cortical bone under mode II loading, employing the End Notched Flexure (ENF) test. The direct method results from the combination of the progress of the mode II strain energy release rate with the crack tip shear displacement, obtained by digital image correlation. The resulting cohesive law is determined by differentiation of this relation relatively to the crack shear displacement. The inverse method employs finite element analyses with cohesive zone modelling, in association with an optimization procedure. The resulting strategy enables determining the cohesive law without establishing a pre-defined shape. The significant conclusion that comes out of this work is that both methods offer consistent results regarding the estimation of the cohesive law in bone. Given that the inverse method dispenses the use of sophisticated equipment to obtain the cohesive law in bone, it can be used as a more convenient procedure to accomplish efficient studies in the context of bone fracture characterization under mode II loading.

© 2018 Published by Elsevier Ltd.

1. Introduction

Fracture characterization of cortical bone is of great interest to those who attempt to model bone damage resulting from accidental involuntary bad falls, road accidents (powerful impact), blast or ballistic trauma [23], as well as those interested to develop material substitutes to mimic bone functions [3], or fabricate prosthetic devices to promote a more adaptive bone remodelling activity (healing) in complex bone fractures [2]. Another area of major interest concerns the development of rigorous techniques to evaluate the fracture risk in bone tissue, as a complementary method to assess bone quality [14]. This important indicator is mostly appropriate in the framework of clinical tests promoted by the pharmaceutical industry, within regular drug delivery protocols. The design of bio-inspired engineering materials presenting higher fracture toughness is also a field of foremost concern, namely for manufacturing exoskeleton structures for many military and civil applications.

Following a very long period of natural selection, bone and bone-like biological tissues (holding an organic matrix and a reinforcement phase, e.g., antler and dentin) have developed a very complex hierarchical microstructure. In fact, similarly to most biological tissues, bone exhibits a microstructure formed by collagen, mineral hydroxyapatite (HA) and water, disposed into distinct length scales: the nanoscale (mineralized collagen fibrils with nanoscopic platelets of HA), the sub microscale (single lamella), the microscale (lamellar structure), the mesoscale (lamellae arranged concentrically around blood vessels, forming osteons) and the macroscale (entire bone) [16]. This material hierarchical arrangement contributes to increase fracture toughness in bone. In fact, when crack propagates in bone tissue, numerous interactions occur between stress singularities and the material microstructure. Because of these interactions, different failure mechanisms can be identified: diffuse microcracking, crack deflection and fibre-bridging [32,33]. These toughening mechanisms are responsible for development of a remarkable fracture process zone (FPZ) leading non-linear fracture mechanics behaviour. The consequence of these failure mechanisms is the development of a pronounced *Resistance*-curve (*R*-curve), in which fracture resistance is defined as a function of crack length as it propagates in a stable manner. Consequently, a valuable option to deal with such nonlinear behaviour is the employment of cohesive zone modelling (CZM). These approaches replicate the development of the significant FPZ typically occurring during bone fracture, by means of a softening law usually called cohesive law (CL). Generally, this softening relationship is assumed *a priori* [6,18,20,28] and the respective cohesive parameters are identified by inverse procedures using global [6,17,19] or local [12,15] data. In the former, the experimental load-displacement (P–δ) curve is fitted numerically through an optimization method. A drawback inherent to this approach lies in the fact that the uniqueness of the obtained solution is not assured, since the fitting is performed employing global data (i.e., P–δ curve). The later aims to reproduce numerically the ex-

---

* Corresponding author.
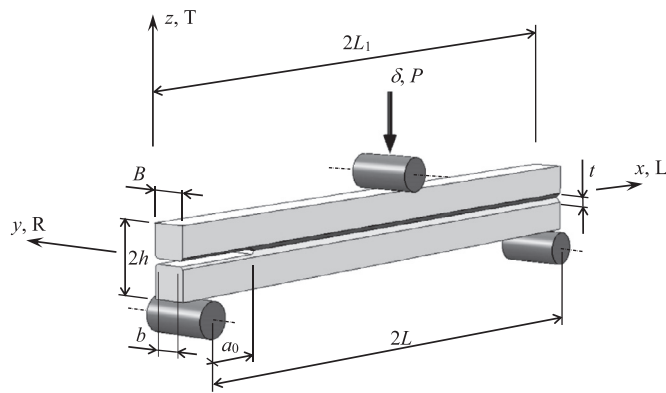 *E-mail address:* famp@utad.pt (F.A.M. Pereira).

Fig. 1. Schematic representation of the ENF test specimen.
($2L_1 = 65$; $2L = 60$; $2h = 6$; $t = 1$, $B \approx 2.5$; $b = 2.3$; $a_0 = 18$ mm).

Fig. 3. Example of a *speckle* pattern.

perimental P–δ curve using the local displacement field measured at the crack by optical methods [5,31]. Alternatively, the CL can be directly obtained combining the experimental P–δ curve with displacement values measured close to the crack tip [1,29]. The last two techniques require high-performance optical equipment and more complex experimental procedures than the former one. In addition, most of these methods require sophisticated optimization algorithms leading to important computational costs.

In this work, the determination of the cohesive law representative of bone fracture under pure mode II loading using the End Notched Flexure (ENF) test is addressed. Two different methods are employed. The direct method is an experimental procedure involving determination of the development of strain energy release rate and crack tip shear displacement. The differentiation of such relation gives rise to the cohesive law. The inverse method was already successfully applied in the context of mode I fracture characterization [21]. It consists in the combination of a finite element analysis including CZM and an optimization method, targeting the minimization of the difference between the numerical and experimental load-displacement curves. A cohesive zone analysis was accomplished aiming to validate the inverse method. The cohesive laws resulting from both methods are compared as well as the advantages and drawbacks of both methods.

2. Experiments

Bovine cortical bone utilized in this work was provided by an accredited local abattoir. Bone femurs were removed from a one day postmortem bovine cadaver local slaughterhouse. Current Portuguese ethical protocols have been scrupulously followed during the specimens'
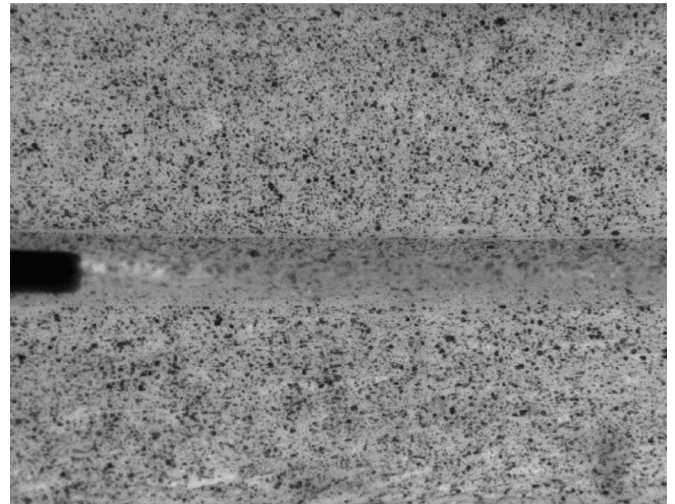
preparation phases. These specimens were shaped from the bulk of femur mid-diaphysis to fit the final dimensions and material orientations shown in Fig. 1 (i.e., longitudinal (L)–transverse (T) plane) and stored at −20° within a gauze immersed in a solution of NaCl (0.9%).

The pre-crack (a_0 in Fig. 1) was executed at the specimen half-height (h) using a fine (0.3 mm thickness) diamond disk along the longitudinal direction. Then, a sharp cutting blade was rigidly tighten to a grip of the testing machine and moved towards the notch root at 100 mm/min, thus inducing a penetration of 0.15 mm. Subsequent to this procedure a V-notch (30°) groove was machined along the specimen length on both sides of the specimen (0.5 mm depth). This method aims to impede crack deflection from the specimen mid-height to assure pure mode II propagation.

Spurious friction in the notched region was reduced by inserting two fine Teflon® bands in the pre-crack, with a thin lubricant layer between them. Fracture tests were performed in a servo-electrical testing machine (Micro Tester INSTRON® 5848) following the setup shown in Fig. 2. The acquisition frequency was set to 5 Hz to register the P–δ curves, employing a 2 kN load-cell. The loading displacement was applied with a rate of 0.5 mm/min to assure stable crack growth. Indentation effects in bone were found negligible, taking into consideration the maximum loads attained during the fracture tests (around 100 N).

The crack tip shear displacement (CTSD) was measured by digital image correlation (DIC) using a speckled pattern painted on the surface of each specimen (matte black ink), before conducting the mechanical test (Fig. 3). The CTSD (i.e., w_{II}) is measured at a pair of equidistant points located close to the crack extremity, being subsequently correlated with

Fig. 2. Testing setup of the ENF test showing the speckle pattern.

Table 1
Components of the optical system and DIC measuring parameters.

CCD camera	
Model	Baumer® Optronic FWX20
	(8 bits, 1624 × 1236 pixels, 4.4 µm/pixel)
Shutter time	1.0 ms
Acquisition frequency	1 Hz
Lens	
Model	Opto Engineering Telecentric lens TC 23 09
Magnification	1.0 ± 3%
Field Of View (1/1.8″)	7.1 mm × 5.4 mm
Working Distance	63.3 ± 2 mm.
Working F-number	11
Field Depth	0.9 mm
Conversion factor	4.0 µm/pixel
Lighting	Raylux® 25 white-light LED
DIC measurements	
Subset size	15 × 15 pixel^2 (0.060 × 0.060 mm^2)
Subset step	13 × 13 pixel^2 (0.052 × 0.052 mm^2)
Resolution	1–2 × 10^{-2} pixel (0.04–0.08 µm)
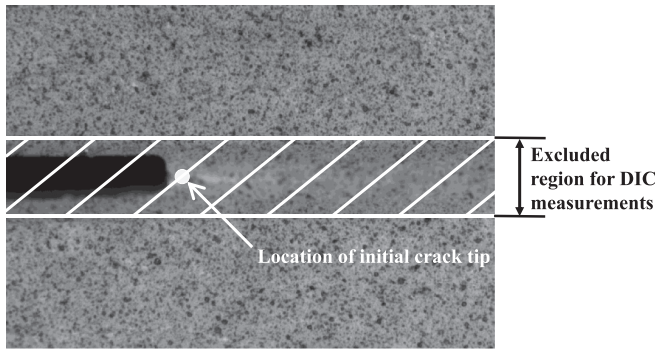
Fig. 4. Image processing.

the applied loading. Table 1 shows the optical components (DIC-2D system from ARAMIS®) and DIC parameters utilized in the process [13,30]. A charge coupled device camera with a telecentric lens (comprising a region of 7.1 × 5.4 mm^2) was used to capture images. The image quality (focus, contrast and appropriate time exposition) was duly controlled acting on the working distance, shutter time and lighting system. High spatial resolution was achieved by choosing a subset size of 15 × 15 pixel^2 (i.e., 0.060 × 0.060 mm^2) and a subset step of 13 × 13 pixel^2 (i.e., 0.052 × 0.052 mm^2). The image quality and precision of measurements were verified by imposing rigid-body translation tests [24,25]. The resolution of the measured displacement is a function of the speckle pattern quality, being in the range of 1–2 × 10^{-2} pixel (i.e., 0.04–0.08 µm) (Table 1).

The presence of the V-shape grooves (dashed region in Fig. 4) leads to poor image quality for DIC measurements. Therefore, the CSTD was performed considering points nearby the crack extremity out of the dashed zone.

3. Identification of cohesive laws (CL)

The CL is a fundamental tool to reproduce materials fracture behaviour with accuracy employing cohesive zone analysis. They establish a constitutive relation between tractions and relative displacements of adjacent integration points of interface finite elements. The determination of the appropriate relation that simulates the fracture response of bone under mode II loading is the objective of the proposed methodology. With this aim, two methods were applied using the ENF experimental test (Fig. 1), specifically the direct approach and the inverse one. The former is based only on experimental data, i.e., on the load-

displacement curve and crack tip shear displacement recorded during the fracture test. The later correlates load-displacement experimental data with a numerical analysis, including CZM governed by a CL with unrestricted shape.

3.1. Direct method

The direct method is based on the following equation

$$G_{\mathrm{II}} = \int_0^{w_{\mathrm{II}}} \sigma_{\mathrm{II}}(w_{\mathrm{II}}^*)\, \mathrm{d}w_{\mathrm{II}}^* \tag{1}$$

which gives the strain energy release rate under pure mode II loading (G_{II}) from the shear traction (σ_{II}) as a function of the crack tip shear displacement (w_{II}) [22]. The mode II cohesive law can be obtained by differentiating Eq. (1) in respect to w_{II}, yielding

$$\sigma_{\mathrm{II}}(w_{\mathrm{II}}) = \frac{\mathrm{d}G_{\mathrm{II}}}{\mathrm{d}w_{\mathrm{II}}} \tag{2}$$

In order to apply this equation to determine the mode II cohesive law, the function $G_{\mathrm{II}} = f(w_{\mathrm{II}})$ should be determined from the experimental data. Hence, G_{II} is evaluated from the P-δ curve obtained during the fracture test, and w_{II} is measured by digital image correlation (DIC). The rigorous evaluation of G_{II} during the fracture test is a fundamental issue. The classical methods are based on specimen compliance calibration or on beam-based theory. Both approaches involve crack length measurement in the course of the test, which is very difficult to be done with the necessary accuracy. In fact, in the ENF fracture tests crack grows with their faces in close contact. In order to surmount this drawback an equivalent crack length procedure previously developed [7], can be followed. The method employs the Timoshenko beam theory to establish the compliance ($C = \delta/P$) versus crack length (a) relation

$$C = \frac{3a^3 + 2L^3}{8\,B\,h^3\,E_{\mathrm{L}}} + \frac{3L}{10B\,h\,G_{\mathrm{LT}}} \tag{3}$$

where E_{L} is the elastic modulus in the longitudinal direction, G_{LT} is the shear modulus of the LT plane and B is the specimen width. The remaining parameters can be identified consulting Fig. 1. Bone is a natural material presenting pronounced scatter in its elastic properties. Owing to this feature, the effective elastic modulus of each specimen (E_f) can be estimated from Eq. (3) using the initial values of crack length (a_0) and compliance (C_0), as follows

$$E_{\mathrm{f}} = \frac{3a_0^3 + 2L^3}{8\,B\,h^3} \left(C_0 - \frac{3L}{10\,B\,h\,G_{\mathrm{LT}}} \right)^{-1} \tag{4}$$

During crack growth, the current compliance C (Eq. (3)) can be used to achieve an equivalent crack length a_e. Therefore, combining Eqs. (3) and (4) yields

$$a_e = \left[\frac{C_c}{C_{0c}} a_0^3 + \frac{2}{3} \left(\frac{C_c}{C_{0c}} - 1 \right) L^3 \right]^{1/3} \tag{5}$$

where

$$C_c = C - \frac{3L}{10\,B\,h\,G_{\mathrm{LT}}} \quad ; \quad C_{0c} = C_0 - \frac{3L}{10\,B\,h\,G_{\mathrm{LT}}} \tag{6}$$

By means of Eqs. (3)–(6) and Irwin–Kies relation

$$G = \frac{P^2}{2\,b} \frac{dC}{da} \tag{7}$$

$G_{\mathrm{II}} = f(a_e)$ can be obtained as follows,

$$G_{\mathrm{II}} = \frac{9\,P^2\,a_e^2}{16\,bBh^3\,E_{\mathrm{f}}} \tag{8}$$

It should be referred that the width of the ligament section is affected by the existence of the longitudinal grooves (Fig. 1). Consequently, the dimension b in Fig. 1 must be considered, instead of the specimen width B.

The presented data reduction scheme provides an easy achievement of the R-curve (i.e., $G_{\mathrm{II}} = f(a_e)$), since it only depends on data resultant
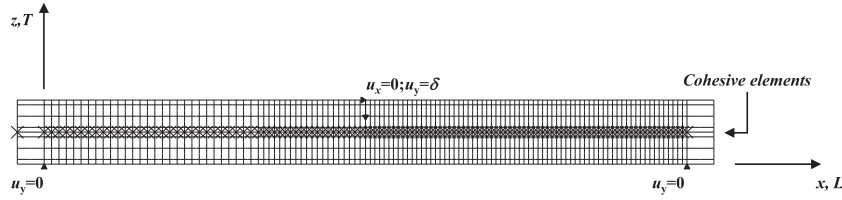
Fig. 5. Finite element mesh used in the ENF test.

Table 2
Nominal mechanical properties of cortical bone [8,9].

E_L (GPa)	E_T (GPa)	G_{LT} (GPa)	ν_{LT}
*	9.55	4.74	0.37

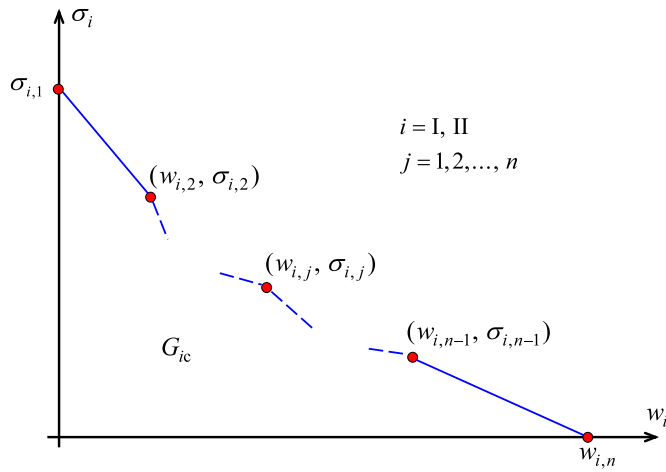* adjusted to each specimen in a trial and error basis.

Fig. 6. Piece-wise cohesive law.

from the load-displacement curve. This strategy avoids the problematic and inaccurate crack length measurement during the test. Moreover, the influence of the energy dissipated in a non-negligible fracture process zone is indirectly taken into account, since the actual specimen compliance is used to find the value of a_e.

3.2. Inverse method

The identification of CL by the developed inverse method is achieved combining an optimization algorithm with finite element analyses (Fig. 5). The used mesh includes 960 isoparametric quadratic plane stress 8-node elements and compatible 120 interface elements to simulate damage onset and propagation. Loading was applied by means of small displacement increments (0.01×2.5 mm) and non-linear geometric analysis was considered. Table 2 presents the elastic properties introduced in the FE model. The longitudinal elastic modulus was adjusted to replicate the linear elastic branch of the P–δ curve obtained experimentally.

The method establishes the profile of the CL, which is assumed to be composed by four linear independent segments (Fig. 6), without any restrictions imposed to the vertices ($w_{II,j}$, $\sigma_{II,j}$, $j = 1, .. 4$). The procedure requires the selection of some points in the experimental load-displacement (P-δ) curve and the assessment of the corresponding energy release rate values in the R-curve (Fig. 7a and b). The selected ajustement points follows the following criterion: the first point is fixed at the nonlinear commencement in the P-δ curve, which corresponds

to damage onset and the subsequent ones are equally spaced in the P–δ curve till the maximum load is attained (near beginning of propagation, i.e., the last point of the CL).

The optimization algorithm intends to minimize the difference between the numerical and experimental loads in the P–δ curves. Hence, for each selected point defined by its applied displacement δ follows,

$$Dif_j = P_j^{num} - P_j^{exp};$$
$$j = 1, 2, 3, 4, 5 \text{ of the } P - \delta \text{ curve} \tag{9}$$

For each iteration k a stress value ($\sigma_{II,k+1}$) is estimated for a given point j, according to the organogram shown in Fig. 8, which presents the *bisection* method [4]. The stress values will be estimated according to the evaluation performed in each point j. Hence, the shear traction value increases (or decreases) if the numerical load underestimates (or overestimates) the experimental one.

For the initial point corresponding to the local strength in the CL (Fig. 6), a different procedure was followed. In fact, the series of traction values providing a good agreement between the numerical and experimental P-δ curves is wide. Consequently, the global response, i.e., the comparison of the entire numerical and experimental P-δ curves, should also be considered in addition to the local difference analysis. This procedure reflects on a further restriction to the model aiming to find a rigorous result. The final step of the procedure consists on the evaluation of the actual relative crack shear displacement. This can be done linking the estimated stress values with the energy release rate values

$$w_{II,j} = \frac{2(G_j - G_{j-1}) + (\sigma_{II,j} + \sigma_{II,j-1}) w_{II,j-1}}{(\sigma_{II,j} + \sigma_{II,j-1})}$$
$$(j = 2, 3, 4, 5) \tag{10}$$

The described procedure provides the estimation of a cohesive law, i.e. $\sigma_{II} = f(w_{II})$, representative of the material damage development under mode II. It must be emphasized that the method is not limited to four branches, although it was verified that this number is enough for a good description for the present case.

4. Cohesive zone model (CZM)

One of the crucial features of the suggested inverse method is the development of a suitable CZM appropriate for bone fracture simulation under mode II loading. Although the ENF is an almost pure mode II fracture test, a mixed-mode cohesive zone model was developed aiming to cover more general loading conditions. The mixed-mode I+II cohesive zone model is based on equivalent quantities combining the two loading modes (I and II). These parameters are the mode ratio (β) and the equivalent values of crack opening displacement (w_m) and traction (σ_m),

$$\beta = w_{II}/w_I \quad w_m = \sqrt{w_I^2 + w_{II}^2} \quad \sigma_m = \sqrt{\sigma_I^2 + \sigma_{II}^2} \tag{11}$$

The cohesive law (CL) to be determined (i.e., $\sigma_m = f(w_m)$) should be able to outline the softening relationship by several consecutive linear sections (Fig. 6). The constitutive equation prior to damage initiation is given by
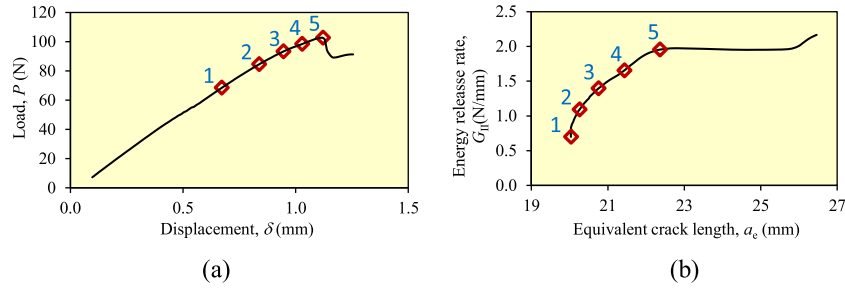
$$\sigma_m = k \, w_m \tag{12}$$

Fig. 7. Points selected for fitting: (a) Load-displacement curve and (b) respective *R*-curve.
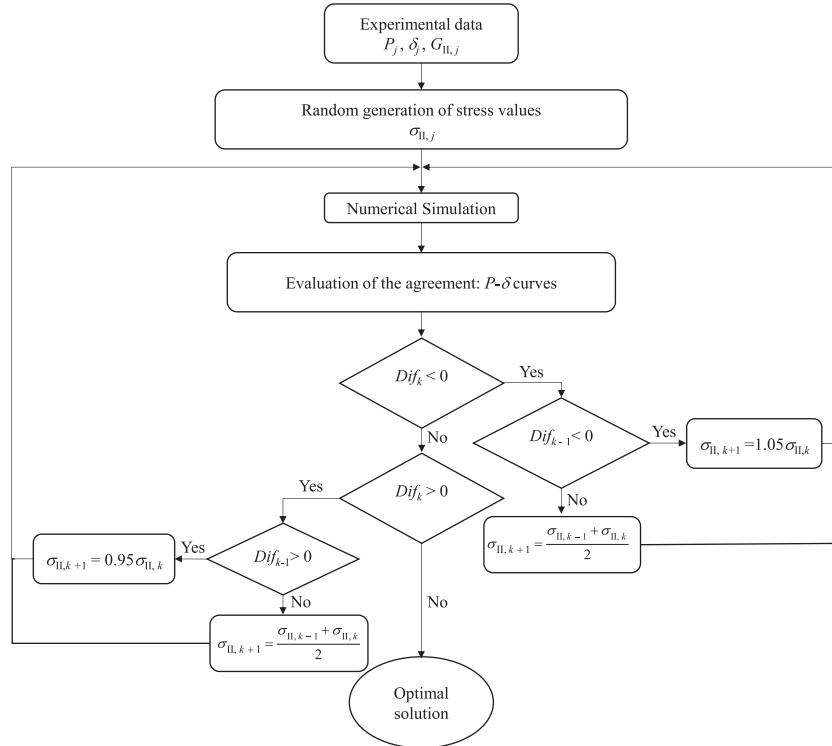

Fig. 8. *Bisection* algorithm ($j = 1, 2, 3, 4,$ and 5 according to Fig. 7).

with k standing for the interfacial stiffness. After damage initiation the constitutive softening relation is described by

$$\sigma_m = (1 - d_m)\,k\,w_m \tag{13}$$

where d_m is the damage parameter varying between zero (undamaged) and one (rupture). Hence, according to the proposed procedure, fracture behaviour of cortical bone was mimicked through a stepwise CL composed by different branches. Therefore, at the inflection points ($j = 1, 2, 3, \ldots n$) (Fig. 6) the equivalent stresses are defined through a quadratic stress criterion

$$\left(\frac{\sigma_I}{\sigma_{I,j}}\right)^{2\alpha} + \left(\frac{\sigma_{II}}{\sigma_{II,j}}\right)^{2\alpha} = 1 \quad \text{if } \sigma_I > 0 \tag{14}$$

$$\sigma_{m,j} = \sigma_{II,j} \quad \text{if } \sigma_I \leq 0$$

where $\sigma_{m,j}$ and $\sigma_{i,j}$ (with $i = I, II$) are, respectively, the mixed-mode I+II traction components and the respective strength values in pure mode loading, at each point j. An analogous relation is employed to determine the crack displacements,

$$\left(\frac{w_I}{w_{I,j}}\right)^{2\alpha} + \left(\frac{w_{II}}{w_{II,j}}\right)^{2\alpha} = 1 \tag{15}$$

After some algebraic manipulations involving Eqs. (11)–(15), the equivalent tractions and crack opening displacements at the inflection points become

$$\sigma_{m,j} = \frac{\sigma_{I,j}\sigma_{II,j}\sqrt{1 + \beta^2}}{\left(\sigma_{II,j}^{2\alpha} + \beta^{2\alpha}\sigma_{I,j}^{2\alpha}\right)^{1/(2\alpha)}} \quad \text{and}$$

$$w_{m,j} = \frac{w_{I,j}w_{II,j}\sqrt{1 + \beta^2}}{\left(w_{II,j}^{2\alpha} + \beta^{2\alpha}w_{I,j}^{2\alpha}\right)^{1/(2\alpha)}} \tag{16}$$

These equivalent quantities are fundamental to establish the growth of the damage parameter as material degradation progresses.

An energetic power law criterion

$$\left(\frac{G_I}{G_{Ic}}\right)^{\alpha} + \left(\frac{G_{II}}{G_{IIc}}\right)^{\alpha} = 1 \tag{17}$$

was considered to simulate damage propagation. Considering that the strain energy release rate is a function of the product between tractions and crack tip displacements, and accounting for Eq. (12), the strain energy release rates mode ratio can be given by $G_{II}/G_I = \beta^2$. Combining
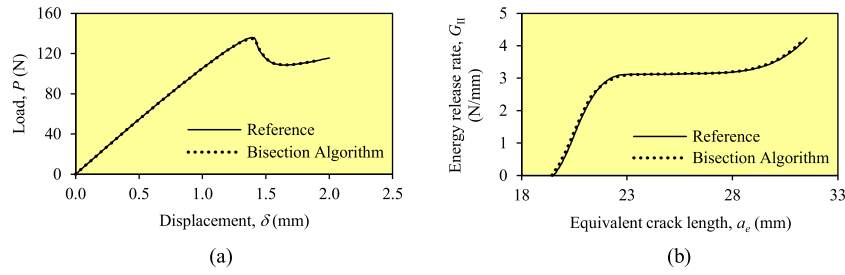
Fig. 9. Comparison between determined and reference (a) P–δ curves and (b) R-curves.

this relation with Eq. (17), the total strain energy release rate for a given mode ratio β yields

$$G_T = G_I + G_{II} = G_I\left(1 + \beta^2\right) = \frac{G_{Ic}G_{IIc}\left(1 + \beta^2\right)}{\sqrt[\alpha]{G_{IIc}^\alpha + \beta^{2\alpha}G_{Ic}^\alpha}} \quad (18)$$

The final relative displacement for $j = n$ (Fig. 6) is determined by equating the total energy (G_T) to the area confined by the mixed-mode I+II stepwise cohesive law, through the equation

$$G_T = \sum_{j=2}^{n} \frac{(\sigma_{m,j} + \sigma_{m,(j-1)})(w_{m,j} - w_{m,(j-1)})}{2} \quad (19)$$

The damage parameter d_m for each piece-wise segment (Fig. 6) can be straightforwardly obtained by making equal the respective softening relationship to $(1 - d_m)k\,w_m$. This procedure yields

$$d_m = 1 - \frac{1}{kw_m}\left[\frac{\sigma_{m,j}\left(w_m - w_{m,(j-1)}\right) + \sigma_{m,(j-1)}\left(w_{m,j} - w_m\right)}{w_{m,j} - w_{m,(j-1)}}\right]$$
$$\text{for } w_{m,(j-1)} \leq w_m \leq w_{m,j} \quad (20)$$

This relation establishes that different softening constitutive relationships (*i.e.*, with different slopes) are being accomplished by the several integration points in the fracture process zone, depending on their position in the CL. In other words, it can be affirmed that damage growth rate depends on the branch of damage evolution.

5. Numerical validation of the inverse method

A validation procedure was performed to prove the soundness of the developed method. Hence, in an initial stage a reference solution was numerically generated. To this end, a combination of cohesive parameters characteristic of cortical bone fracture was considered to mimic bovine cortical bone damage onset and propagation (labelled as Reference in Fig. 6; $w_{II,2} = 0.018$ mm, $\sigma_{II,2} = 59.5$ MPa, $G_{IIc} = 3.13$ N/mm). Then, the FE modelling (Fig. 5) of the ENF test was performed to obtain the reference P-δ curve (Fig. 9a). Applying the CBBM (Eqs. (5) and ((8)), the mode II fracture energy release rate (G_{II}) in function of the equivalent crack length (i.e., the Reference R-curve in Fig. 9b) is obtained. These numerical P-δ and R-curves are then used as the reference solution to be reproduced by the inverse method. Hence, the numerical P-δ curve identified as the Reference (Fig. 9a) was taken as the "experimental" result, whose CL might be identified. Thus, a set of points (a total of 5) were chosen according to the criterion referred in the previous section (Fig. 7a).

The process starts with random generation of the stress values ($\sigma_{II,j}$ in Fig. 8). Iterative FE simulations of the ENF test performed in the optimization procedure provide an excellent agreement relatively to the experimental P-δ curve (Fig. 9a) using the CL represented in Fig. 10 (identified as Bisection Algorithm). The R-curve resulting from FE analysis using this CL was compared with the one ensuing from the "experimental" P–δ curve. The observed overall excellent agreement validates
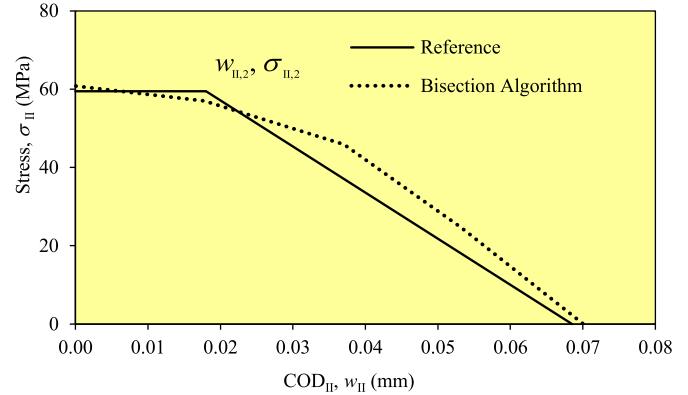

Fig. 10. Comparison between determined cohesive law and the one used as input.

the proposed procedure, as it proved to be very effective to determine the CL.

6. Analysis and discussion of results

The accurate determination of bone cohesive laws requires that self-similar crack propagation during the fracture test is assured. The adopted experimental conditions have been effective in this test, since damage propagation occurred in the specimen half-height due to the machined lateral grooves (see arrows in Fig. 11a–c). The clear misalignment observed between specimen arms at the notched root (represented by w_{II} in Fig. 11d), is an evidence that shear loading is predominant in this test.

Figs. 12 (a–c) show an example of the agreement achieved between the numerical curve obtained by the inverse method and the direct one for a given specimen. Hence, Fig. 12a and b reveal that fine agreement was obtained for the load-displacement and R-curves, respectively. The resulting cohesive laws (Fig. 12c) identified by the direct method (denoted as Experimental) and the inverse method (denoted as Numerical) reveal some difference although the global trend is in agreement. These results highlight the capability of the proposed procedures to reproduce with accuracy the mode II fracture phenomenon in cortical bone.

Fig. 13(a–b) plot the ensemble of the cohesive laws obtained by the employed methods. The CLs resulting from the direct method reveal some difficulty for the lower displacement values (close to zero) owing to resolution limitation of the DIC technique.

The detailed results can be consulted in Table 3. The average values of $w_{II,n}$ provided by both methods are in close agreement. The average shear strengths reveal that the inverse method value is 13.7% higher than the one obtained with the direct method. Nevertheless, the results obtained by the two methods were compared using the test-t. In light of this, the two results were considered statistically equivalent. In addition, the values of shear strength in bone were compared to values given in literature. Although most of them refer to human cortical bone (Table 4)
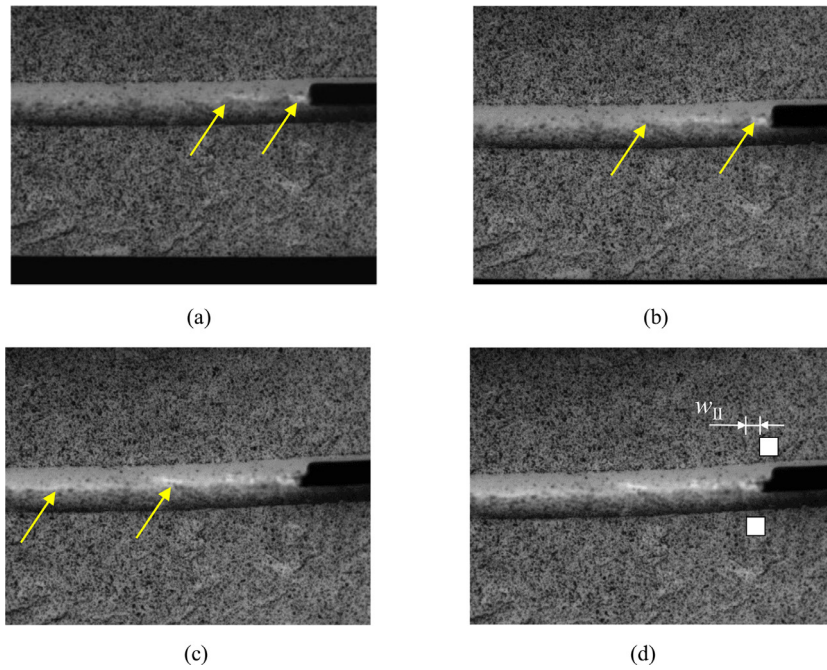
Fig. 11. Damage development: (a) initial phase, (b) in-between phase, (c) maximum load and (d) noticeable propagation (specimen 17).
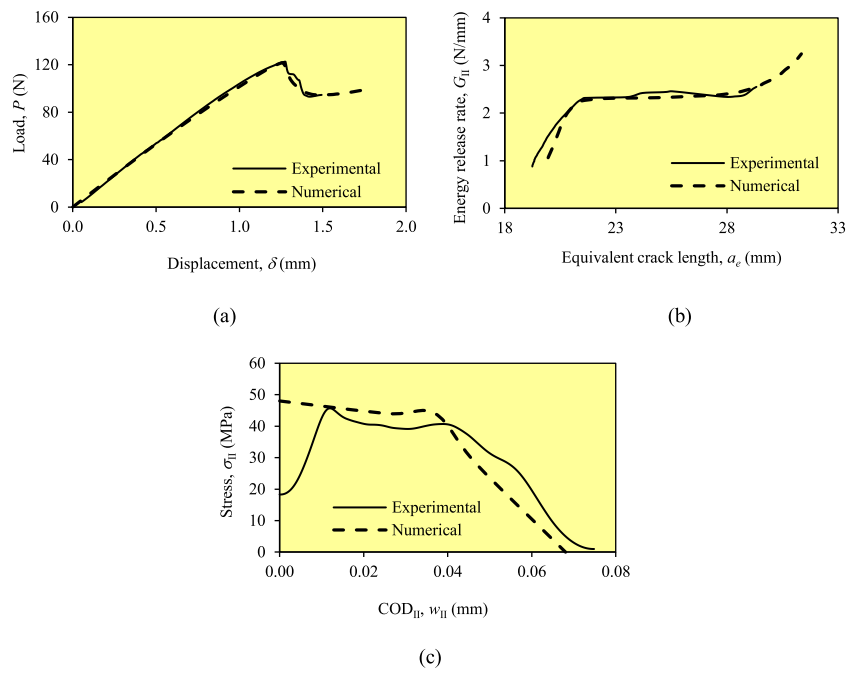

Fig. 12. Comparison between the experimental (direct method) and numerical curve identified by the inverse optimization method: (a) P–δ curves, (b) R-curves, (c) Cohesive laws (specimen 14 in Table 3).
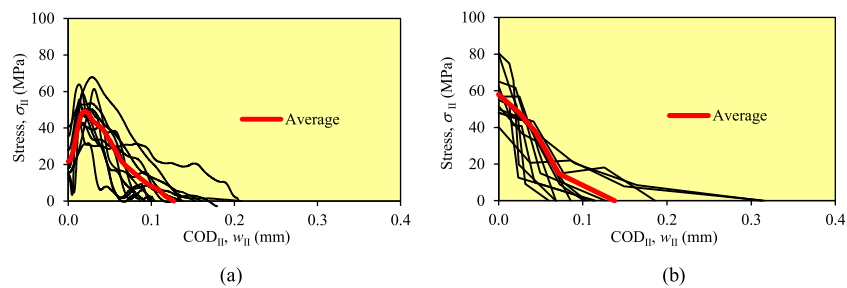

Fig. 13. Mode II cohesive laws obtained by the (a) direct method and (b) inverse method.

Table 3

Experimental results: $\sigma_{II,1}$, ultimate cohesive shear strength; $w_{II,c}$, maximum mode II opening displacement; $G_{law,II}$, fracture energy evaluated from de cohesive law.

Specimen Number	Experimental			Numerical	
	$\sigma_{II,1}$ (MPa)	$w_{II,n}$ (mm)	$G_{law,II}$ (N/mm)	$\sigma_{II,1}$ (MPa)	$w_{II,n}$ (mm)
1	50.32	0.16	3.49	40.16	0.32
2	63.90	0.10	3.05	65.00	0.13
3	59.24	0.09	2.69	50.00	0.10
4	55.61	0.10	2.13	80.53	0.07
5	43.13	0.09	1.30	55.00	0.02
6	45.65	0.10	2.34	48.00	0.07
7	67.88	0.21	5.25	58.09	0.31
8	46.85	0.14	2.39	62.35	0.11
9	42.81	0.12	2.93	51.62	0.10
10	51.70	0.06	1.92	80.00	0.06
11	53.65	0.15	3.54	56.81	0.10
12	31.41	0.21	4.55	48.00	0.28
Average	51.01	0.13	2.97	57.96	0.14
CoV(%)	19.7	37.4	37.6	21.4	74.2

Table 4

Values of shear strengths found in other works.

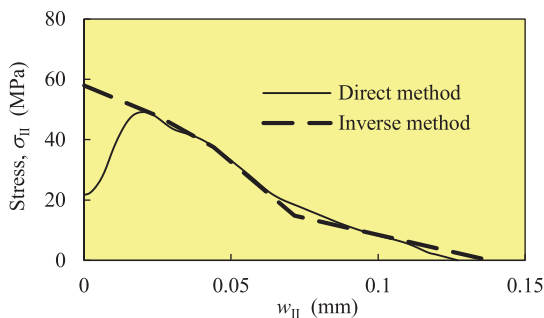| Work	Bone type	Experimental test	$\sigma_{II,1}$ (MPa)
[27]	Human femur	Iosipescu	51.6 ± 1.90
[10]	Human tibia	Inclined double notch shear	61.4 ± 6.30
[11]	Bovine femur	Inverse method	59.5 ± 6.30
[26]	Human femur	Iosipescu	49.9 ± 6.20

Fig. 14. Average mode II cohesive laws obtained by the direct and inverse methods.

it can be settled that they are similar to the ones obtained in the present work.

A final comparison between average cohesive laws obtained by direct and inverse procedures is shown in Fig. 14. The initial part of the cohesive laws reveal a discrepancy which is induced by the specificities of the utilized methods. Anyway, an excellent agreement has been obtained in the softening region characterizing the fracture process. This result reveals the soundness of the inverse procedure.

7. Conclusions

The aim of the present work was to determine the cohesive law of bovine cortical bone under mode II loading using the ENF test. Two different methods were developed with this aim. The direct method is an experimental procedure based on the correlation between the development of the strain energy release rate under mode II loading (G_{II}) and the

crack tip shear displacement (CTSD) monitored by digital image correlation. Owing to difficulties inherent to crack length identification during the ENF test, an equivalent crack length based data reduction scheme was employed to get the evolution of G_{II}. The cohesive law results from differentiation of the $G_{II} = f(CTSD)$ relation. The inverse method is, basically, a numerical procedure involving finite element analysis with cohesive zone modelling and an optimization algorithm. The objective is to determine the cohesive law that minimizes the difference between numerical and experimental load-displacement curves. The softening relationship is assumed to be described by a polyline with several branches without any restrictions in the shape of the law. The inverse method was validated by a numerical analysis including a cohesive zone modelling.

Comparing the ensuing cohesive laws provided by the two methods it can be settled that both procedures give rise to consistent results, meaning that they can be efficaciously utilized to evaluate cohesive laws representative of mode II fracture of bovine cortical bone. In fact, they produce comparable results, meaning that the inverse procedure is valid. This is a quite interesting achievement, since estimations of the cohesive laws can be done in an easier post-processing analysis of simple experimental data, without requiring specific equipment, as is the case of DIC analysis necessary in the direct method.

Conflict of interests

The authors testify that there are no conflict of interests with the content of this paper.

Acknowledgments

References

[1] Andersson T, Biel A. On the effective constitutive properties of a thin adhesive layer loaded in peel. Int J Fract 2006;141:227–46.

[2] Bougherara H, Bureau MN, Yahia LH. Bone remodeling in a new biomimetic polymer-composite hip stem. J Biomed Mater Res, Part A 2010;92A:164–74.

[3] Campana V, Milano G, Pagano E, Barba M, Cicione C, Salonna G, Lattanzi W, Logroscino G. Bone substitutes in orthopaedic surgery: from basic science to clinical practice. J Mater Sci Mater Med 2014;25:2445–61.

[4] Chapra SC, Canale RP. Numerical methods for engineers: with personal computer applications. New York: McGraw-Hill; 1985.

[5] Chen X, Deng X, Sutton MA, Zavattieri P. An inverse analysis of cohesive zone model parameter values for ductile crack growth simulations. Int J Mech Sci 2014;79:206–15.

[6] Cox BN, Yang Q. Cohesive zone models of localization and fracture in bone. Eng Fract Mech 2007;74:1079–92.

[7] de Moura MFSF, Silva MAL, de Morais AB, Morais JJL. Equivalent crack based mode II fracture characterization of wood. Eng Fract Mech 2006;73:978–93.

[8] Dempster WT, Coleman RF. Tensile strength of bone along and across the grain. J Appl Phys 1961;16:355–60.

[9] Dong XN, Guo XE. The dependence of transversely isotropic elasticity of human femoral cortical bone on porosity. J Biomech 2004;37:1281–7.

[10] Dong XN, Luo Q, Wang X. Progressive post-yield behavior of human cortical bone in shear. Bone 2013;53:1–5.

[11] Dourado N, Pereira FAM, de Moura MFSF, Morais JJL, Dias MIR. Bone fracture characterization using the end notched flexure test. Mater Sci Eng C 2013;33:405–10.

[12] Ferreira MDC, Venturini WS, Hild F. On the analysis of notched concrete beams: from measurement with digital image correlation to identification with boundary element method of a cohesive model. Eng Fract Mech 2011;78:71–84.

[13] GOM mbH (2007). ARAMIS DIC 2D/3D. Commercial software.

[14] Greenwood C, Clement JG, Dicken AJ, Evans JPO, Lyburn ID, Martin RM, Rogers KD, Stone N, Adams G, Zioupos P. The micro-architecture of human cancellous bone from fracture neck of femur patients in relation to the structural integrity and fracture toughness of the tissue. Bone Reports 2015;3:67–75.

[15] Hong S, Kim KS. Extraction of cohesive-zone laws from elastic far-fields of a cohesive crack tip: a field projection method. J Mech Phys Solids 2003;51:1267–86.

[16] Kataruka A, Mendu K, Okeoghene O, Puthuvelil J, Akono A-T. Microscopic assessment of bone toughness using scratch tests. Bone Reports 2017;6:17–25.

[17] Maier G, Bocciarelli M, Fedele R. Some innovative industrial prospects centered on inverse analyses. Parameter Identification of Materials and Structures. CISM Int Centre Mech Sci 2005;469:55–93 2005.

[18] Morais JJL, de Moura MFSF, Pereira FAM, Xavier J, Dourado N, Dias MIR, Azevedo JMT. The double cantilever beam test applied to mode I fracture characterization of cortical bone tissue. J Mech Behav Biomed Mater 2010;3:446–53.

[19] Oh JC, Kim HG. Inverse estimation of cohesive zone laws from experimentally measured displacements for the quasi-static mode I fracture of PMMA. Eng Fract Mech 2013;99:118–31.

[20] Pereira FAM, Morais JJL, de Moura MFSF, Dourado N, Dias MIR. Evaluation of bone cohesive laws using an inverse method applied to the DCB test. Eng Fract Mech 2012;96:724–36.

[21] Pereira FAM, de Moura MFSF, Dourado N, Morais JJL, Xavier J, Dias MIR. Direct and inverse methods applied to the determination of mode I cohesive law of bovine cortical bone using the DCB test. In Press. Int J Solid Struct 2017;128:1–11.

[22] Rice JR. A path independent integral and the approximate analysis of strain concentration by notches and cracks. J Appl Mech 1968;35:379–86.

[23] Shannahan L, Weerasooriya T, Gunnarsson A, Sanborn B, Lamberson L. Rate-dependent fracture modes in human femoral cortical bone. Int J Fract 2015;194:81–92.

[24] Sousa AMR, Xavier J, Morais JJL, Filipe VMJ, Vaz M. Processing discontinuous displacement fields by a spatio-temporal derivative technique. Opt Lasers Eng 2011;49:1402–12.

[25] Sousa AMR, Xavier J, Vaz M, Morais JJL, Filipe VMJ. Cross-correlation and differential technique combination to determine displacement fields. Strain 2011;47:87–98.

[26] Tang T, Ebacher V, Cripton P, Guy P, McKay H, Wang R. Shear deformation and fracture of human cortical bone. Bone 2015;71:25–35.

[27] Turner CH, Wang T, Burr DB. Shear strength and fatigue properties of human cortical bone determined from pure shear tests. Calcif Tissue Int 2001;69:373–8.

[28] Ural A, Vashishth D. Cohesive finite element modeling of age-related toughness loss in human cortical bone. J Biomech 2006;39:2974–82.

[29] Valoroso N, Sessa S, Lepore M, Cricrì G. Identification of mode-I cohesive parameters for bonded interfaces based on DCB test. Eng Fract Mech 2013;104:56–79.

[30] Xavier J, de Jesus AMP, Morais JJL, Pinto JMT. Stereovision measurements on evaluating the modulus of elasticity of wood by compression tests parallel to the grain. Constr Build Mater 2012;26:207–15.

[31] Xu Y, Li X, Wang X, Liang L. Inverse parameter identification of cohesive zone model for simulating mixed-mode crack propagation. Int J Solids Struct 2014;51:2400–10.

[32] Yeni YN, Norman TL. Calculation of porosity and osteonal cement line effects on the effective fracture toughness of cortical bone in longitudinal crack growth. J Biomed Mater Res 2000;51:504–9.

[33] Zioupos P. Recent developments in the study of failure of solid biomaterials and bone: fracture and prefracture toughness. Mat Sc Eng C 1998;6:33–40.